

MEASUREMENTS OF THE WORK FUNCTION OF SINGLE-WALLED CARBON NANOTUBES ENCAPSULATED BY AgI, AgCl, AND CuBr USING KELVIN PROBE TECHNIQUE WITH DIFFERENT KINDS OF PROBES

A. A. Zhukov ^{a*}, M. V. Chernysheva ^b, A. A. Eliseev ^b

^a Institute of Solid State Physics, Russian Academy of Science
142432, Chernogolovka, Moscow Region, Russia

^b Department of Materials Science, Moscow State University
119991, Moscow, Russia

Received June 22, 2015

We report the results on the measurements of the work function of single-walled carbon nanotubes encapsulated by AgI (AgI@SWCNT), AgCl (AgCl@SWCNT), and CuBr (CuBr@SWCNT) by the local Kelvin probe technique. We found the values of the work function of tubes encapsulated with AgI and AgCl ($\Phi(\text{AgI@SWCNT}) = 5.08 \pm 0.02$, $\Phi(\text{AgCl@SWCNT}) = 5.10 \pm 0.02$ eV) to exceed substantially that of pristine carbon nanotubes, and the value of the work function of carbon nanotubes encapsulated with CuBr is $\Phi(\text{CuBr@SWCNT}) = 4.89 \pm 0.03$ (eV). The measurements are carried out using different kinds of microscope probes including multi-walled carbon nanotube tips.

DOI: 10.7868/S0044451016070154

1. INTRODUCTION

Since the discovery of carbon nanotubes [1], essential efforts have been invested into investigation and characterization of the peculiarities of electronic transport in such structures [2]. Ballistic one-dimensional transport, the four-fold degeneracy of energy levels, spin-orbit coupling, etc. result in reach physics phenomena exhibited by single-walled carbon nanotubes (SWCNTs) [2].

Besides the investigations of pristine SWCNTs, a new branch devoted to chemically modified single-walled carbon nanotubes emerged recently [3]. While most of the experiments on the electronic structure of these objects were performed using traditional optics and X-rays spectroscopy techniques, pioneering investigations of their electronic transport properties have also been done [4–8]. An event of greatest promis was the demonstration of the very stable *p*–*n* diode characteristics of partially encapsulated SWCNTs even in air conditions [7,8]. Unfortunately, characterization of the

band structure of these devices was carried out by measuring nonlinear electronic transport of the whole system. No local investigations of the doped and undoped parts of the diode have been reported so far. On the other hand, further development of electronic components based on chemically modified SWCNTs necessitates knowledge of their internal band and chemical structure.

This issue can be solved by two scanning probe techniques: the local Kelvin probe [9–14] and the scanning gate microscopy applied in linear and nonlinear regimes [15–18]. Both methods have established themselves as being extremely efficient for investigations of the local properties of low-dimensional nanostructures. Kelvin probe microscopy was widely used for experimental determination of the electronic properties of pristine carbon nanotubes and carbon-nanotube-based field-effect transistors [11–14].

The first local characterization of the work function of encapsulated carbon nanotubes on SiO₂ substrates was reported in 2009 [10]. The measurements were performed in almost ambient conditions, with the arm to simulate a typical operating environment of an intra-nanotube *p*–*n* junction and analyze the effect of the CuI dopant on the value of the SWCNT work function. The

* E-mail: azhukov@issp.ac.ru

crucial role of low relative humidity in avoiding the formation of a water film on the sample surface, masking and essentially reducing the doping effect, was reported [10]. The difference in the work function (WF) value of 0.1 eV for doped and pristine SWCNTs allows easily detecting and localizing encapsulate atoms [10].

Among the dopants enabling a high (up to 70 %) SWCNT loading and provisional modification of the carbon nanotube WF over 0.2 eV, chemical compounds such as CuCl, CuBr, AgCl, AgBr, and AgI are of special interest for practical applications [19, 20]. To date, experimental WF values have been reported for CuCl@SWCNT, $\Phi(\text{CuCl@SWCNT}) = 5.25$ eV, and CuBr@SWCNT, $\Phi(\text{CuBr@SWCNT}) = 5.2$ eV, as measured by X-ray photoelectron spectroscopy for massive samples [20]. The WF of SWCNTs encapsulated by AgI was measured using the Kelvin probe technique: $\Phi(\text{CuCl@SWCNT}) = 5.12$ eV [21]. A diamond-coated tip (DCP 11, NT-MDT) was used in the experiments.

In this paper, we present the results on local measurements of the WF of SWCNTs encapsulated by AgI (AgI@SWCNT), AgCl (AgCl@SWCNT), and CuBr (CuBr@SWCNT). Measurements were performed in almost ambient conditions similar to those in [10] using atomic-force microscope tips of different kinds including tips made of multi-walled carbon nanotubes. The Kelvin probe scan resolutions for different tip types were compared. Advantages of the use of multi-walled carbon nanotube tips in Kelvin probe techniques, including in the example of visualization of the water film formation on the sample surface, are presented and discussed as well.

This paper is organized as follows: in Sec. 2, we describe sample preparation, SWCNT growth, and doping procedures and give a detailed description of the scanning method and the microscope tips used; in Sec. 3, we present experimental results and a discussion; Sec. 4 contains our conclusions.

2. EXPERIMENTAL DETAILS

Single-walled carbon nanotubes were formed by the catalytic arc-discharge method using graphite rods 0.8 cm in diameter with Y/Ni powder catalyst at the 73.3 kPa helium pressure and a current of 100–110 A. The SWCNTs were purified by a multistage procedure consisting in controllable oxygenation in air and rinsing by HCl for the catalyst removal. To form halide intercalated SWCNTs, the purified and pre-opened nanotubes (0.025g) were ground with corresponding water-free salts (Aldrich, 99 wt%) in the mass ratio 1 : 0.5,

evacuated to 10^{-5} mbar for 1 h, and sealed into a quartz ampoule. The samples were treated at a temperature of 100 °C above the melting point of corresponding halide for 6 h and slowly cooled (0.02 °C/min) to room temperature to induce better crystallization of the guest compounds inside SWCNTs [22]. Necessary experimental details can be found in [19, 20].

Single-walled carbon nanotubes encapsulated by AgI, AgCl, and CuBr have been thoroughly investigated using Raman spectroscopy, high-resolution X-ray photoelectron near-edge X-ray absorption fine-structure spectroscopy, optical absorption, and high-resolution transmission electron microscopy [19, 20]. All dopants were identified as acceptors. Additionally, it was shown that charge transfer increased in the sequence CuI < CuBr < CuCl due to the increased electron affinity of the halogen atoms [19]. While AgCl demonstrates an amorphous structure inside nanotubes, AgI and CuBr form nanocrystals according to high-resolution transmission electron microscopy data [19, 20].

The specimens for Kelvin probe measurements were prepared on standard *p*-type doped silicon/silicon oxide wafers. The thickness of the SiO₂ layer was 1000 nm. The silicone substrate served as a back gate. On the surface of SiO₂, metallic (Pd) contact mesh was formed by optical lithography [10].

The samples of encapsulated nanotubes were dispersed in isopropanol using an ultrasonic bath and then disposed on the substrate surface. Lithography processing was performed prior to the carbon nanotube deposition to prevent a possible influence of the residual photoresist on the value of the WF of carbon nanotubes [23].

Three types of atomic-force microscopy tips were used for Kelvin probe measurements: two commercially available cantilevers from NT-MDT¹⁾ and a self-made multi-walled carbon nanotube tip, prepared in accordance with the procedure reported in [24].

Kelvin probe measurements [9] were performed in the dual scan mode. During the first scan, topography information was obtained; on the second scan, the potential in the Kelvin probe mode was registered. For Kelvin probe measurements, the AC voltage at the resonance frequency of the cantilever (f_0) and a DC voltage were applied to the conductive cantilever and mechanical oscillations of the cantilever were detected with a photodiode. The feedback signal was adjusted

¹⁾ We used commercially available scanning probe microscope cantilevers DCP11 (diamond coated, typical radius is 70 nm) and NSG11 (NSG11/W2C series, typical radius is 35 nm) by NT-MDT.

by a DC voltage to maintain the amplitude of cantilever oscillations equal to zero. The applied DC voltage was recorded during the second scan. A typical height of the tip above the sample surface on the second run was kept in the range 30 to 60 nm.

Because the Kelvin probe signal represents the WF difference between the tip and the sample surface, an additional calibration of the experimental setup was performed on Pd contacts with the known WF.

The measurements of the lever arm parameter $\alpha = (dC_{CNT}/dz)/(dC/dz)$, where dC_{CNT}/dz and dC/dz are the differential tip-to-nanotube capacitance and the total differential tip capacitance, were carried out in accordance with [25]. During this experiment, the back gate voltage was kept constant at $V_{BG} = 0$ and the AC voltage $V_{AC} = 20$ mV was applied at the frequency $f = 121$ Hz to the palladium mesh contacting SWCNTs. During the Kelvin probe scan run, the response signal from the cantilever was preliminarily filtered from the resonance frequency of the cantilever (f_0). The filtered signal was demodulated by a phase-lock loop, using an external lock-in amplifier (Signal Recovery, model 7225), and then recorded by the microscope electronics instead of the Kelvin probe signal during this run. In our experimental setup, standard NT-MDT electronics allows obtaining a stable and reliable signal from the cantilever in the Kelvin probe feed-back locked regime up to $f = 160$ Hz when $V_{AC} = 20$ mV is applied. Similarly to [25], the resulting signal measured over the nanotubes and far from the Pd mesh (δV_{AC}) allows extracting the value of the level arm $\alpha = \delta V_{AC}/V_{AC}$. The measurements of the lever arm were done at the same heights as the Kelvin probe scans.

Measurements of the WF of carbon nanotube samples were done in air conditions at a relative humidity $RH < 10\%$. According to paper [10], the absence of the water film on the sample surface is crucial for measuring the unmasked value of the WF. As we show in this paper, it is possible to directly visualize the water film formation at $RH > 10\%$ using a carbon nanotube tip. The precision of the extracted WF values is ± 0.02 eV.

3. EXPERIMENTAL RESULTS AND DISCUSSION

Figure 1 illustrates the typical topography (Fig. 1a) and Kelvin probe microscopy scans (Fig. 1b) for the AgI@SWCNT composite acquired using a commercially available NSG11/W2C (NT-MDT) tip coated by TiN (typical radius 35 nm). Two sections of a single-

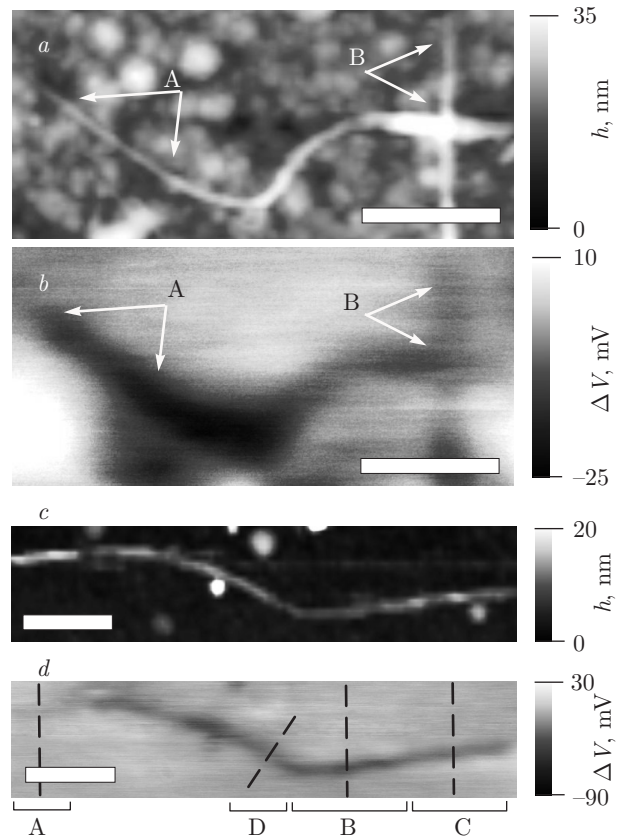


Fig. 1. *a, b:* topography and Kelvin probe scans for an AgI@SWCNT sample acquired with an NSG11/W2C tip. Sections A and B in Figs. *a* and *b* are marked with arrows. *c, d* topography and Kelvin probe scans for an AgCl@SWCNT sample acquired with a multi-walled carbon nanotube tip. Positions of the cross cuts of sections A to D are shown with dashed lines. Horizontal scale bars in each scan are 0.5 μ m in length

walled carbon nanotube are marked as “A” and “B” in Fig. 1a. According to Kelvin probe measurements (Fig. 1b), these sections have essentially different values of the WF: 4.96–4.98 eV for section “A” and 5.06–5.10 eV for section “B”. These two sections can be easily identified as pristine or slightly doped (section “A”) and AgI@SWCNT (section “B”). The WF values were extracted using the lever arm parameter $\alpha \approx 0.12$ measured experimentally [25, 26].

The extracted WF value $\Phi(\text{AgI@SWCNT}) = 5.08 \pm 0.02$ eV stays in quite a good agreement with the value $\Phi(\text{AgI@SWCNT}) \approx 5.12$ eV obtained earlier by the Kelvin probe technique using a diamond-coated tip (DCP 11 by NT-MDT) [21]. The increase in the WF for AgI-doped nanotubes in comparison with pristine ones illustrates acceptor-type doping [20].

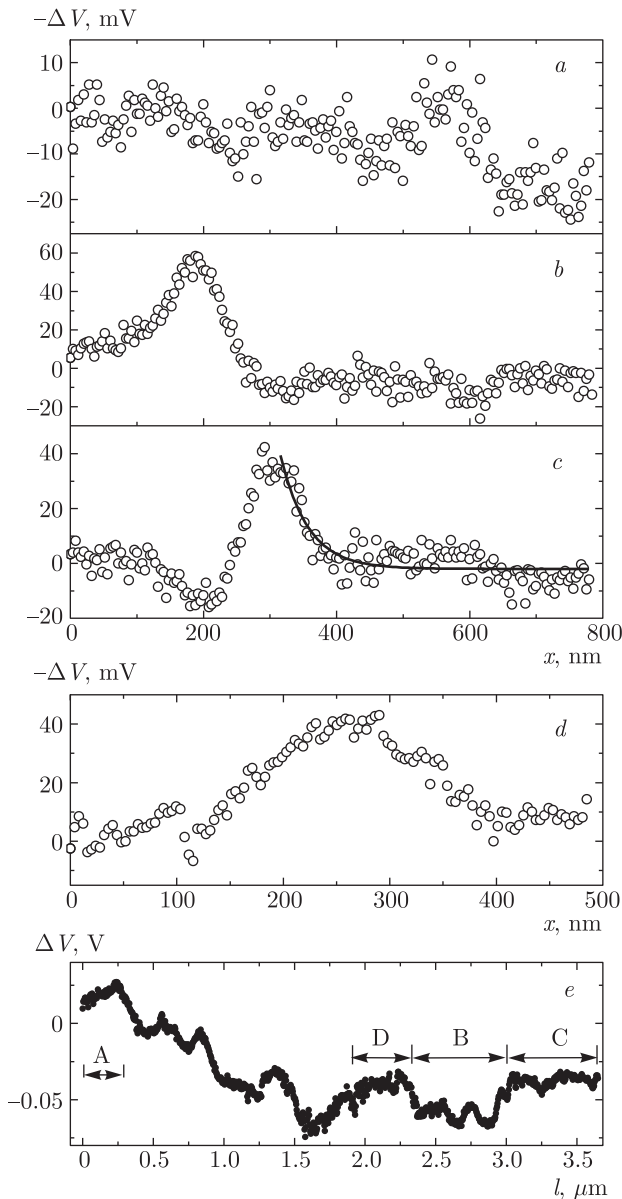


Fig. 2. *a–d:* results of the cross cuts for sections A to D (see Fig. 1c and 1d) of the potential profile of the AgCl@SWCNT sample measured with a multi-walled carbon nanotube tip. The solid line in Fig. c is exponential function $\exp(-(x-x_0)/l_t)$, where $l_t = 45$ nm is a characteristic length of signal decay. *e:* the result of a cross cut along the tube of the potential profile (see Fig. 1c and 1d). Sections A to D are marked

The topography and Kelvin probe microscopy scans for the AgCl@SWCNT composite are presented in Fig. 1c and d. The data were obtained using a multi-walled carbon nanotube tip. A much better resolution for both scans is well seen by unaided eye. Results of the four cross cuts of sections “A” to “D” and a profile

along the tube are shown in Fig. 2*a–e*. The positions of the cross cuts are marked with dashed lines. The extracted WF values are $\Phi_{C,D} = 5.10 \pm 0.02$ eV for sections “C” and “D”, $\Phi_B = 4.90 \pm 0.02$ eV for section “B”, and $\Phi_A \approx 5.3$ eV for section “A”. Among others, section “B” represents a minimal value and can be identified as a pristine or slightly doped single-walled carbon nanotube bundle [10], while sections “C” and “D” can be assigned to AgCl@SWCNT bundles with the obtained value of the WF $\Phi(\text{AgCl@SWCNT}) = 5.10 \pm 0.02$ eV. It is worth noting that the diameter of the bundle at section “D” is less than 4 nm, which corresponds to a bundle containing 3 to 4 nanotubes, while the one at cross section “C” is 8 nm in diameter. The value of the lever arm parameter $\alpha \approx 0.12$ measured experimentally was used in the calculations [25, 26].

The obtained value $\Phi_A \sim 5.3$ eV for section “A” must be discussed in some more detail. The diameter of a bundle for section “A” is 12–14 nm, and we can therefore speculate that the measured value can result from overdoping the single-walled carbon nanotubes with dopant species contained in between the SWCNTs. These species unlikely can occur in bundles consisting of several nanotubes, considering the essential effort made to eliminate any dopant outside SWCNTs during sample preparation [20].

As in the case of AgI, encapsulation by AgCl results in acceptor doping of nanotubes with a slightly more pronounced effect of charge transfer. This is in agreement with the data presented previously based on photoemission experiments [20] and also resemble the sequence of doping effects in a row of halides [20].

The observed sections of single-walled carbon nanotubes hundreds of nanometers in length with a nearly constant WF allows confirming the statement that the sample preparation technique is good enough to create the encapsulated single-walled carbon nanotubes for field-effect transistors and further electronic transport experiments.

The line in cross section C in Fig. 2c shows the exponential decay function $\exp(-(x-x_0)/l_t)$, where l_t is a characteristic length of signal decay and $x_0 = 300$ nm is the position of the single-walled carbon nanotube bundle. This approximation helps to estimate the spatial resolution of the Kelvin probe technique in our experiment for a multi-walled carbon nanotube tip. The obtained value $l_t \approx 45$ nm is essentially less than the previously reported value of 170 nm [25]. Such an improvement in the spatial resolution is quite remarkable considering the use of a specially redesigned ULTRASHARP tip (Micromash) for previous studies [25].

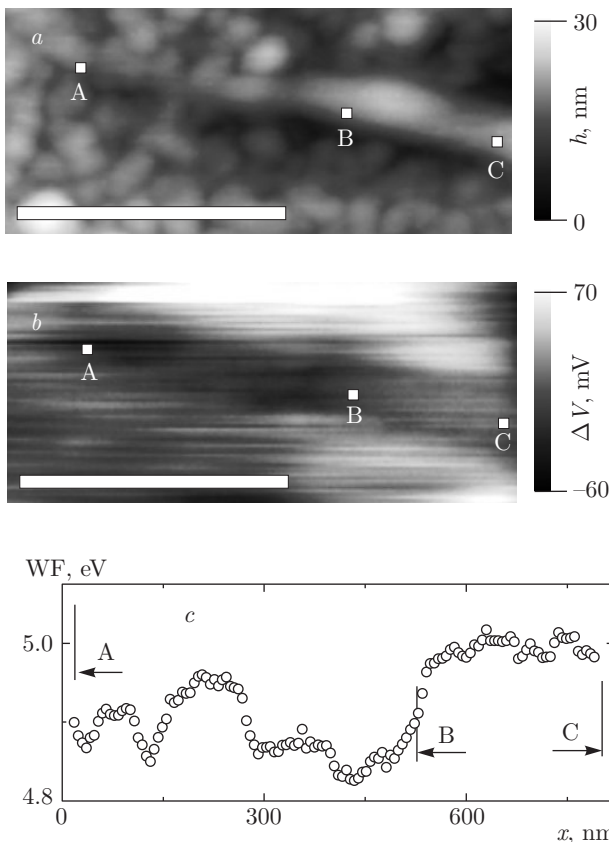


Fig. 3. *a*: a topography image of a CuBr intercalated SWCNT sample measured with a DCP11 tip. *b*: Kelvin probe measurement of the same area. *c*: the value of the WF recalculated from the Kelvin probe image cross-cut section from point A to point C. Horizontal scale bars in each scan are 0.5 \$\mu\text{m}\$ in length

Figure 3 shows the topography, a Kelvin probe microscopy scan, and a cross section of the Kelvin probe scan made along the “A”–“B”–“C” line for a CuBr@SWCNT sample. These measurements were performed using a DCP 11 tip with a typical radius of 70 nm. Experimental values of the lever arm parameter $\alpha \approx 0.15$ and 0.16 measured for the respective “A”–“B” and “B”–“C” sections were used in the WF calculation [25, 26]. The measured value $\Phi \approx 5.0$ eV for a single-walled carbon nanotube bundle 20 nm in diameter (a section from point “B” to “C” in Fig. 3) indicates that this bundle contains slightly doped single-walled carbon nanotubes. According to Fig. 3*c*, this value is quite stable along the whole thickness of the bundle section. The rest of the bundle with a diameter below 10 nm (from point “A” to “B”) exhibits a much less stable value of the WF ranging from 4.83 eV to 4.96 eV. At the bundle tail close to point “A”, where its diameter decreases below 2 nm and the bundle might

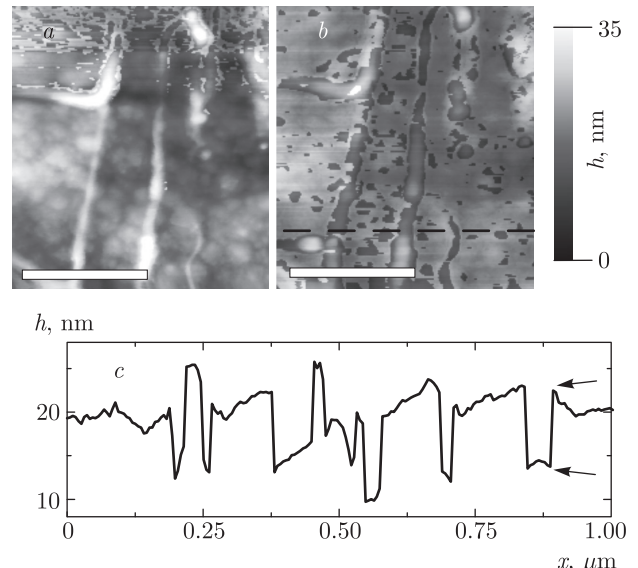


Fig. 4. *a* and *b*: topography of an AgCl@SWCNT sample measured with a multi-walled carbon nanotube tip. The “long scan” direction is perpendicular to the dashed line in Fig. *b*. The scan goes from bottom up in both images. The relative humidity is 10 % at the beginning of scan *a* and 15 % at the end of the scan. For scan *b*, the value of relative humidity starts from 15 % and increases to 25 % at the end of the scan (the top of the image). *c*: a cross-cut section of scan *b* marked with the dashed line. Arrows in Fig. *c* mark the step due to the film formation. The step size is around 9 nm. Horizontal scale bars in both scans are 0.5 \$\mu\text{m}\$ in length

contain a single SWCNT only, the WF is 4.89 ± 0.03 eV. This result is much less than the previously reported value $\Phi(\text{CuBr@SWCNT}) = 5.2 \pm 0.1$ eV measured by a photoemission technique [19]. Besides the ambient conditions of the Kelvin probe experiment setup, the disagreement can be explained by the high diversity of WF values within a massive sample, which results in an effective WF increase in large nanotube bundles due to the contact potential equalization [27]. Additional experiments using the photoemission electron microscopy technique to locally resolve the response of a single nanotube are required [28].

Figures 4*a* and 4*b* present the experimental data of the measured topography of an AgCl@SWCNT sample using a multi-walled carbon nanotube tip. The “long-time” scan direction is along the Y coordinate and perpendicular to the dashed line in Fig. 4*b*. The starting value of relative humidity is RH = 10 % at the beginning of the scan (the bottom of the image in Fig. 4*a*). Gradually increasing, the relative humidity reaches the value RH = 15 % at the end of the scan (the top of the image). For the scan in Fig. 4*b*, relative humidity in-

creases from RH = 15 % to RH = 25 %. The formation of “lakes” with a marge height of around 9 nm is clearly visible. The additional steps are marked with arrows in Fig. 4c, and the position of this cross-cut section is marked with the dashed line in Fig. 4b. Water film formation essentially reduces the spatial resolution of a topography image. Decreasing the relative humidity to 10 % restores the initial spatial resolution of the topography completely. Thus, maintaining a value $\text{RH} \leq 10\%$ is necessary for reliable and nonmasked WF measurements.

It was not possible to extract an extra adhesive force of the water film in our experimental setup similarly to [29–32] because no well-defined and reproducible hysteresis in spectroscopy measurements done on the surface covered with a water film was observed. This is probably because of the lack of stiffness of the multi-walled nanotube itself and a nonperfect mechanical tip-to-carbon-nanotube connection (the tube is not glued). Nevertheless, the visualization of the water film formation is an additional essential reason for the application of multi-walled carbon nanotube tips in local measurements of the WF, besides an ultimate spatial resolution and the overall robustness of such a kind of tips.

4. CONCLUSION

We performed local measurements of the WF of a single-walled carbon nanotube encapsulated by AgI, AgCl, and CuBr using the Kelvin probe technique. Measurements were done with different types of atomic-force microscope tips including multi-walled carbon nanotubes as the least invasive one with the ultimate spacial resolution. The obtained values of the local WF of encapsulated carbon nanotubes $\Phi(\text{AgI@SWCNT}) = 5.08 \pm 0.02$ eV and $\Phi(\text{AgCl@SWCNT}) = 5.10 \pm 0.02$ eV are slightly less than those reported by the photoemission technique for bulk samples. The local WF for an individual CuBr@SWCNT filament $\Phi(\text{CuBr@SWCNT}) = 4.89 \pm 0.03$ eV was less than the WF measured previously for a bulk sample [19], indicating the necessity of local measurements for a further understanding of the SWCNT doping by encapsulated materials.

Using multi-walled carbon nanotube tips, the possibility to visualize and check the process of water film formation at $\text{RH} > 12\%$ has also been shown. This observation involves an additional reason for the application of multi-walled carbon nanotube tips in Kelvin probe experiments.

SWNTs were synthesized by A. V. Krestinin, Institute of Problems of Chemical Physics, RAS, Chernogolovka, Russia. The authors thank V. Dremov and A. Grebenko for the technical support with the multi-walled carbon nanotube tip preparation. This work is supported by the Russian Foundation for Basic Research, programs of the Russian Academy of Science, the Program for Support of Leading Scientific Schools, and Russian Science Foundation (grant No. 14-13-00747).

REFERENCES

1. S. Iijima, Nature **354**, 56 (1991).
2. J.-Ch. Charlier, X. Blase, and S. Roche, Rev. Mod. Phys. **79**, 677 (2007).
3. A. Eliseev, L. Yashina, M. Kharlamova, and N. Kiselev, in: *Electronic Properties of Carbon Nanotubes*, ed. by J. M. Marulanda, InTech (2011), p. 127, ISBN 978-953-307-499-3.
4. B. W. Smith, M. Monthioux, and D. E. Luzzi, Nature (London) **396**, 323 (1998).
5. S. Okada, M. Otani, and A. Oshiyama, Phys. Rev. B **67**, 205411 (2003).
6. T. Takenobu, T. Takano, M. Shiraishi, Y. Murakami, M. Ata, H. Kataura, Y. Achiba, and Y. Iwasa, Nature Mater. **2**, 683 (2003).
7. Y. F. Li, R. Hatakeyama, J. Shishido, T. Kato, and T. Kaneko, Appl. Phys. Lett. **90**, 173127 (2007).
8. T. Kato, R. Hatakeyama, J. Shishido, W. Oohara, and K. Tohji, Appl. Phys. Lett. **95**, 083109 (2009).
9. M. Nonnenmacher, M. P. O’Boyle, and H. K. Wickramasinghe, Appl. Phys. Lett. **58**, 2921 (1991).
10. A. A. Zhukov, V. K. Gartman, D. N. Borisenko, M. V. Chernysheva, and A. A. Eliseev, JETP **109**, 307 (2009).
11. X. Cui, M. Freitag, R. Martel, L. Brus, and Ph. Avouris, Nano Lett. **3**, 783 (2003).
12. Yu. Miyato, K. Kobayashi, K. Matsushige, and H. Yamada, Jpn. J. Appl. Phys. **44**, 1633 (2005).
13. T. Umesaka, H. Ohnaka, Yu. Ohno, S. Kishimoto, K. Maezawa, and T. Mizutani, Jpn. J. Appl. Phys. **46**, 2496 (2007).
14. G. Riu, A. Verdaguer, F. A. Chaves, I. Martin, P. Godignon, E. Lora-Tamayo, D. Jimenez, and F. Perez-Murano, Microelectron. Eng. **85**, 1413 (2008).

15. M. A. Topinka, B. J. LeRoy, S. E. J. Shaw et al., *Science* **289**, 2323 (2000).
16. J. L. Webb, O. Persson, K. A. Dick, C. Thelander, R. Timm, and A. Mikkelsen, *Nano Research* **7**, 877 (2014).
17. D. Martin, A. Heinzig, M. Grube, L. Geelhaar, Th. Mikolajick, H. Riechert, and W. M. Weber, *Phys. Rev. Lett.* **107**, 216807 (2011).
18. S. R. Hunt, E. J. Fuller, B. L. Corso, and P. G. Collins, *Phys. Rev. B* **85**, 235418 (2012).
19. A. A. Eliseev, L. V. Yashina, N. I. Verbitskiy, M. M. Brzhezinskaya, M. V. Kharlamova, M. V. Chernysheva, A. V. Lukashin, N. A. Kiselev, A. S. Kumskov, B. Freitag, A. V. Generalov, A. S. Vinogradov, Y. V. Zubavichus, E. Kleimenov, and M. Nachtegaal, *Carbon* **50**, 4021 (2012).
20. A. A. Eliseev, L. V. Yashina, M. M. Brzhezinskaya, M. V. Chernysheva, M. V. Kharlamova, N. I. Verbitsky, A. V. Lukashin, N. A. Kiselev, A. S. Kumskov, R. M. Zakalyuhin, J. L. Hutchison, B. Freitag, and A. S. Vinogradov, *Carbon* **48**, 2708 (2012).
21. A. A. Zhukov, V. K. Gartman, and A. A. Eliseev, “Nanophysics and Nanoelectronics. XV International Conference” **1**, 255 (2011).
22. M. V. Chernysheva, A. A. Eliseev, A. V. Lukashin, Yu. D. Tretyakov, S. V. Savilov, N. A. Kiselev, O. M. Zhigalina, A. S. Kumskov, A. V. Krestinin, and J. L. Hutchison, *Physica E: Low-Dimensional Systems and Nanostructures* **37**, 62 (2007).
23. H. Hosoi, M. Nakamura, Y. Yamada et al., *J. Physics: Conference Series* **100**, 052085 (2008).
24. V. Dremov, V. Fedoseev, P. Fedorov, and A. Grebenko, arXiv.cond-mat:1406.5117v2.
25. E. J. Fuller, D. Pan, B. L. Corso, O. Tolga Gul, J. R. Gomez, and Ph. G. Collins, *Appl. Phys. Lett.* **102**, 083503 (2013).
26. D. Brunel, D. Deresmes, and Th. Melin, *Appl. Phys. Lett.* **94**, 223508 (2009).
27. J. Zhao, J. Han, and J. Ping Lu, *Phys. Rev. B* **65**, 193401 (2002).
28. E. Bauer, M. Mundschau, W. Sweich, and W. Telieps, *Ultramicroscopy* **31**, 49 (1989).
29. X. Xiao and L. Qian, *Langmuir* **16**, 8153 (2000).
30. M. He, A. S. Blum, D. E. Aston, C. Buenaviaje, R. M. Overney, and R. Luginbuehl, *J. Chem. Phys.* **114**, 1355 (2001).
31. L. Sirghi, *Appl. Phys. Lett.* **82**, 3755 (2003).
32. J. Grobelny, N. Pradeep, D.-I. Kim, and Z. C. Ying, *Appl. Phys. Lett.* **88**, 091906 (2006).